A rapid screening of Ru(II) photosensitizers

Pierre G. Potvin,* Phuong Uyen Luyen and Fahad Al-Mutlaq

Department of Chemistry, York University, 4700 Keele Street, Toronto, ON, Canada M3J 1P3. E-mail: pgpotvin@yorku.ca; Fax: +1 416 736 5936

Received (in New Haven, CT, USA) 11th December 2000, Accepted 2nd March 2001
First published as an Advance Article on the web 1st May 2001

When samples containing a Ru(II)-based photosensitizer such as $Ru(bpy)_3^{2+}$ (bpy is 2,2′-bipyridine), methyl viologen (MV^{2+}) and the sacrificial reductant triethanolamine (TEOA) are exposed to white light, the blue colour of the methyl viologen cation radical ($MV^{\bullet+}$) develops by oxidative quenching of the sensitizer's excited state. This occurs even if the samples are not degassed, that is in spite of the known quenching of $MV^{\bullet+}$ by O_2. In degassed media, however, a second pathway of $MV^{\bullet+}$ formation occurs, known to involve the reduction of MV^{2+} by the oxidized and deprotonated form of TEOA ($H_{-1}TEOA^{\bullet}$) that arises from its function as a sacrificial reductant. This second pathway masks the effect of the photosensitization and disallows comparative analyses, but is suppressed by O_2. The second pathway also interferes in aqueous media, as the O_2 content becomes diffusion-limited. In order to comparatively assess the utility of Ru(II) photosensitizers, a method is described that uses non-degassed samples in CH_3CN under continuous irradiation with spectrophotometric monitoring of $MV^{\bullet+}$. This requires little sample preparation and simple equipment, and is applicable to sensitizers with widely varying excited state lifetimes. A kinetic model that takes account of the aerobic quenching furnishes rate constants relating to $MV^{\bullet+}$ formation and (non-aerobic) quenching that are reproducible, consistent with mechanistic expectations and concordant with the sensitizer excited state lifetime. The rate constants can then be used to compare sensitizers subject to the same oxidative quenching.

Ru^{II} complexes continue to elicit much interest as photosensitizers, for instance in solar storage applications such as the photo-generation of H_2 from H_2O.[1] In order to launch a combinatorial search of organo-soluble sensitizers to be embedded in membranes in imitation of the photosynthetic reaction centre,[2] we required a rapid method of assessing the usefulness of large numbers of sensitizer preparations in organic media.

One possible approach is to photophysically characterize the sensitizers and their photo-induced reactions using Stern–Volmer and transient absorption analyses,[3] but this requires carefully controlled conditions, specialized equipment and a number of experiments for an assessment of each sensitizer. Another approach is to quantitatively monitor stable photoproducts. For instance, Kalyanasundaram *et al.* described the photosensitization of H_2 evolution by $Ru(bpy)_3^{2+}$ (bpy is 2,2′-bipyridine) in aqueous solutions containing PtO_2, methyl viologen (MV^{2+}) as an oxidative quencher and electron relay, and triethanolamine (TEOA).[4] The latter serves as sacrificial reductant to reduce the Ru^{III} photoproduct, thereby regenerating the sensitizer and inhibiting the wasteful reverse reaction of Ru^{III} with the other photoproduct, the methyl viologen cation radical ($MV^{\bullet+}$). The $MV^{\bullet+}$ then survives to transfer an electron to the Pt catalyst where the reduction of H^+ occurs. Other H_2 generation systems have been described[5,6] though the co-generation of O_2 remains elusive. Setting aside the issues of catalyst choice, deactivation[7,8] and pH dependence, the adaptation of such H_2 production for our purposes would require the accurate measurement of small gas volumes with specialized equipment. As have some other authors,[9–14] we instead pursued the more direct approach of spectrometrically measuring the accumulation of $MV^{\bullet+}$.

This paper describes such measurements, using CH_3CN solutions without degassing, simple equipment and no special protection of the detector from stray irradiation, for two sensitizers possessing very different photophysical properties, and demonstrates how the kinetic parameters governing the process can be obtained and used to compare sensitizers.

Results

Although $MV^{\bullet+}$ is known to be unstable in air,[4] we found that non-degassed CH_3CN or H_2O solutions of $Ru(bpy)_3^{2+}$, MV^{2+} and TEOA slowly turned blue, the characteristic colour of $MV^{\bullet+}$, upon exposure to sunlight. This indicated that the aerobic quenching of $MV^{\bullet+}$ by O_2 did not prevent its accumulation, and we devised a protocol for its measurement (described in the Methodology section). Using similar concentrations of these reagents in CH_3CN as in the aqueous H_2-generation system of Kalyanasundaram *et al.*,[4] we were able to reproducibly monitor the build-up of $MV^{\bullet+}$ in a disposable cuvette without degassing and under continuous irradiation from a slide projector. Fig. 1 presents the time course of the $MV^{\bullet+}$ absorbance at 600 nm (A^{600}) in typical runs. The A^{600} rose quickly, then leveled off to reach a maximum within 35 s, during which time the solution became a strong blue. The presence of $MV^{\bullet+}$ was confirmed by comparison of the spectrum of the irradiated sample with literature data.[4] The steady-state A^{600} level could be maintained for extended periods if the irradiation was continued but, after removing the light source, A^{600} decayed smoothly within about 300 s to return to its original value, owing to aerobic quenching. Such a growth–decay cycle could be repeated several times with the same sample without significant difference in the A^{600} curves, and the steady-state radical concentrations ($[MV^{\bullet+}]_{\infty}^{obs}$) achieved were reproduced with other samples of the same sensitizer with standard deviations of about 11% among them. As also shown in Fig. 1, $MV^{\bullet+}$ generation was observed even with the much poorer sensitizer $Ru(ttpy)_2^{2+}$ where Hpy is 4′-*p*-tolyl-2,2′ : 6′,2″-terpyridine [triplet-state lifetime $\tau = 0.95$ ns[15] *vs.* 680 ns[16] with $Ru(bpy)_3^{2+}$]. It was slower and stopped at a lower but fairly reproducible $[MV^{\bullet+}]_{\infty}^{obs}$ value (9% stan-

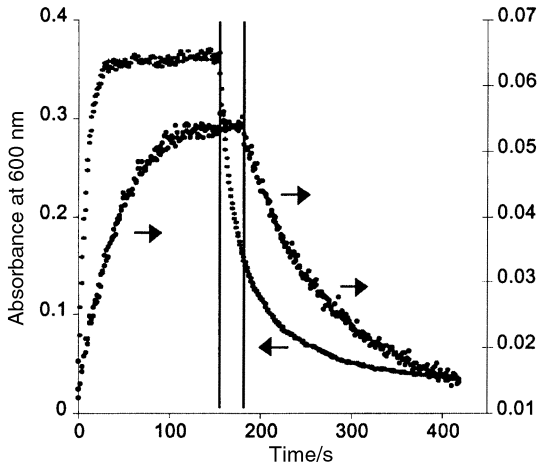

Fig. 1 Plots of A^{600} against time with $[Ru(bpy)_3](PF_6)_2$ (upper plot, left-hand scale) and with $[Ru(ttpy)_2](PF_6)_2$ (lower plot, right-hand scale). The vertical lines mark the time when irradiation was stopped. *Conditions*: 4×10^{-5} M sensitizer, 9.45×10^{-3} M $MV(PF_6)_2$ and 0.05 M TEOA in CH_3CN at room temperature.

dard deviation). Using 2,2′ : 5′,2″-terthiophene sensitizers, Kim *et al.* described a similar growth–steady state–dark decay cycle.[14]

Although the $MV^{\bullet+}$ yields are already a rough measure of the sensitizer efficiency, this is subject to the vagaries of aerobic decay at uncontrolled O_2 concentrations. We therefore developed a kinetic model that took account of the aerobic decay in order to provide rate constants relating to $MV^{\bullet+}$ formation that can be used in comparisons between sensitizers.

The dark A^{600} decay curves were found to be second-order in $[MV^{\bullet+}]$ over their entirety, with weak first-order contributions. Thus, they obeyed

$$\left\{\frac{d[MV^{\bullet+}]_t}{dt}\right\}_{dark} = -k_{d1}[MV^{\bullet+}]_t - k_{d2}[MV^{\bullet+}]_t^2 \qquad (1)$$

where k_{d1} and k_{d2} are *pseudo*-first- and second-order rate constants, respectively. These were determined with ppm accuracy by non-linear fits. The value of k_{d2} varied from 1317 to 2849 $M^{-1}\ s^{-1}$ while k_{d1} varied from 0 to $2.916 \times 10^{-3}\ s^{-1}$. With the stronger sensitizer, k_{d1} was negligibly weak (on the order of $10^{-8}\ s^{-1}$ or less). Even with $Ru(ttpy)_2^{2+}$ samples developing the lowest concentrations of $MV^{\bullet+}$ (near 5 μM), the second-order contribution was dominant, at least initially. We found no relationship between the measured k_{d1} and k_{d2} values and the former could be neglected with little effect on subsequent calculations (see below). As expected, the more important k_{d2} varied from sample to sample {with standard deviations of 3.7% over three independently assembled samples of $[Ru(bpy)_3]^{2+}$, 3.9% with $[Ru(ttpy)_2]^{2+}$}, and from cycle to cycle with any one sample but in a *time-independent* manner {with standard deviations of 2.9–10.4% over three cycles with $[Ru(bpy)_3]^{2+}$, 5.4–8.0% with $[Ru(ttpy)_2]^{2+}$}, suggesting that $[O_2]$ was roughly constant in any one sample, not diffusion-limited and in excess. The lower signal-to-noise ratios in the weaker $[Ru(ttpy)_2]^{2+}$ data accounts for the greater variations and uncertainties in their analyses.

The irradiated A^{600} growth curves were found to obey the following rate law, which includes the aerobic decay terms,

$$\frac{d[MV^{\bullet+}]_t}{dt} = k_f[MV^{2+}]_t - (k_q + k_{d1})[MV^{\bullet+}]_t - k_{d2}[MV^{\bullet+}]_t^2$$

$$= k_f[MV^{2+}]_0 - (k_f + k_q + k_{d1})[MV^{\bullet+}]_t - k_{d2}[MV^{\bullet+}]_t^2 \qquad (2)$$

and where k_f and k_q are pseudo-first-order rate constants for the cation radical growth and quenching by Ru^{III}, respectively. Mechanistic models that generate the observed rate laws are presented in the Discussion section. Values of k_f and k_q for any one growth cycle were assessed using the k_{d1} and k_{d2} values estimated from the subsequent dark decay cycle as the best available estimates of the effect of aerobic decay during the irradiation phase. This gave excellent fits, as described in the Methodology section. (As also detailed there, it was not possible to treat k_{d1} and k_{d2} as variables.) With any one sample, the variation in k_f was small {$\leqslant$3.7% over three cycles with $[Ru(bpy)_3]^{2+}$, $\leqslant$3.9% with $[Ru(ttpy)_2]^{2+}$}. The value of k_f was only weakly affected by a neglect of k_{d1}. The variation in k_q was usually stronger {$\leqslant$6.3% over three cycles with the same sample of $[Ru(bpy)_3]^{2+}$; $\leqslant$7.3% with $[Ru(ttpy)_2]^{2+}$} and understandably more sensitive to a neglect of k_{d1}. In computations where k_{d2} was artificially varied, the numerical correlation between k_{d2} and k_f was weak ($\delta k_f/k_{d2} = -3.32 \pm 0.03 \times 10^{-8}$ M) but k_q was a thousand-fold more strongly correlated ($\delta k_q/k_{d2} = -3.25 \pm 0.04 \times 10^{-5}$ M). With k_{d1} and k_{d2} set at the dark decay values, the resultant k_q values from multiple samples showed no residual correlation with the sample-specific k_{d2} values, but were correlated with k_f (see later). Hence, this approach provides measures of k_q that are independent of aerobic decay rates and O_2 concentrations.

Table 1 gathers the experimental averages of k_f and k_q and expresses the averaged $[MV^{\bullet+}]_\infty^{obs}$ values as percent yields χ^{obs}. The relatively small uncertainties in the k parameters attest to the small sample-to-sample variations and the kinetic analysis can be said to give consistent results.

To lend further support to our analysis, we varied the concentration of each component over an order of magnitude. We found that (i) increasing either $[MV^{2+}]_0$ or $[Ru(bpy)_3]_0^{2+}$ caused increases in k_f, k_q and a net increase in $[MV^{\bullet+}]_\infty^{obs}$, while (ii) increasing $[TEOA]_0$ caused no change in k_f, a decrease in k_q and a net increase in $[MV^{\bullet+}]_\infty^{obs}$. The former finding is consistent with previous findings[9,13] and with the known roles of the sensitizer and the electron relay, in that more sensitizer will lead to more of the excited state, and therefore to more $MV^{\bullet+}$, while an increase in $[MV^{2+}]_0$ will allow more effective trapping of the excited state and thus more $MV^{\bullet+}$. At the same time, both effects lead to higher k_q values because both serve to also produce more of the Ru^{III} co-product, which in turn can quench $MV^{\bullet+}$ more effectively. Indeed, the numerical correlation between k_f and k_q values reflects this mechanistic link. The effect of varying $[TEOA]_0$ was also consistent with previous findings[13] and with the known function of TEOA, that is to not participate in the generation of $MV^{\bullet+}$ but to reduce the concentration of the co-generated Ru^{III} and thus inhibit the quenching. Hence, our kinetic model provides results consistent with the accepted oxidative quenching mechanism operating in this system.

To be useful in comparisons between sensitizers, the kinetic analyses need to also reflect photosensitizer ability. For assessment purposes, we employed another measure of utility, the $MV^{\bullet+}$ yield achievable in an O_2-free system, given by

$$\chi^{theor} = \frac{[MV^{\bullet+}]_\infty^{theor}}{[MV^{2+}]_0} = \frac{k_f}{k_f + k_q}$$

an expression obtained by applying the steady-state assumption to eqn. (2) with k_{d1} and k_{d2} both set to 0. This, unlike χ^{obs},

Table 1 Results averaged over three samples run through three averaged growth–decay cycles. Weighted uncertainties in the least significant digits are given in brackets

	$Ru(bpy)_3^{2+}$	$Ru(ttpy)_2^{2+}$
χ^{obs} (%)	0.42(5)	0.092(8)
$k_{init}/10^{-4}\ s^{-1}$	2.65(7)	0.0936(4)
$k_f/10^{-4}\ s^{-1}$	3.02(5)	0.1081(4)
$k_q/10^{-2}\ s^{-1}$	3.06(4)	0.84(3)
χ^{theor} (%)	0.98	0.13

is an intrinsic measure free from the vagaries of variable O_2 concentrations (and variable k_d values). The expectations are that a better sensitizer will show higher k_f and χ^{theor} values and, because k_f and k_q are mechanistically linked, a higher k_q value as well, but not necessarily a higher χ^{obs}. The calculated χ^{theor} values are included in Table 1. Not only can $MV^{\bullet+}$ be reliably measured with sensitizers of vastly different τ values, the kinetic analyses also provided results consistent with this difference: the sensitizer with the longest-lived excited state formed $MV^{\bullet+}$ fastest and in greatest quantity. Moreover, it was associated with the higher k_q value, and would theoretically achieve the highest $[MV^{\bullet+}]_\infty^{obs}$ in an O_2-free environment.

While a sensitizer's τ value is but one determinant of its ability (others include λ_{max}, ε, E°_{ox}),[1] the two sensitizers used here differ most significantly in their τ values and otherwise have a similar constitution and similar spectral and redox properties. Okura and Kim-Thuan employed graphical estimates of the instantaneous rate of $MV^{\bullet+}$ formation but were able to similarly correlate those estimates with the τ values of $Ru(bpy)_3{}^{2+}$ and three Ru^{II} phenanthroline complexes.[9] The τ-based comparison made here serves to validate the kinetic model but does not preclude the use of the model to compare sensitizers differing in other respects.

For comparison, we also assessed the initial rates of $MV^{\bullet+}$ growth over the first 5 s of irradiation, and calculated the initial rate constants k_{init} (=initial rate/$[MV^{2+}]_0$). These systematically underestimated k_f but were reasonably well correlated with them. The sample-averaged k_{init} values are included in Table 1. Their ratio matched the k_f ratio very well. Being simpler to compute than k_f values, they might also be useful indicators of sensitizer ability if they are measured in a consistent manner.

Samples were also run after a thorough degassing in a specially designed cuvette, and, as expected, the known interference by a TEOA-derived radical[4] led to very different results. Two runs at different sensitizer concentrations are illustrated in Fig. 2. Both show an initial curvilinear growth phase, much like that seen in the aerobic samples, followed by a linear region of growth that raised A^{600} to much higher levels than achieved earlier. The rate of rise in A^{600} then sloped off, by which time it had reached the instrument's detection limit and had become exceedingly noisy. The absorption spectrum measured at this point under irradiation again confirmed the presence of $MV^{\bullet+}$. Turning the light source off did not result in a decay of A^{600}, and the sample

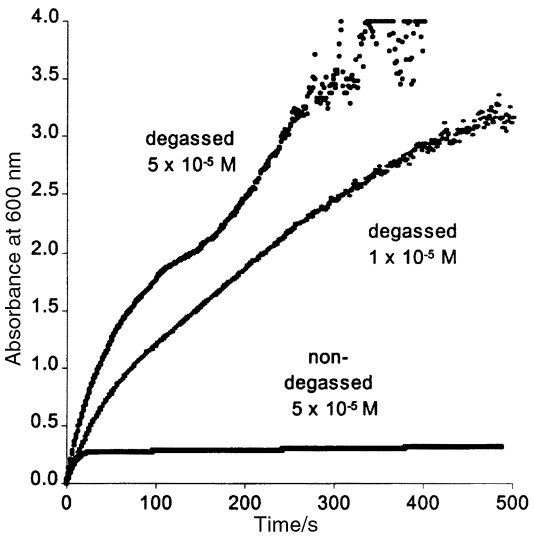

Fig. 2 Plots of A^{600} over time with degassed samples of $[Ru(bpy)_3]^{2+}$ at the indicated concentrations and state. These solutions in CH_3CN also contained 0.006 M $MV(PF_6)_2$ and 0.05 M TEOA.

remained deep blue.† Upon the admission of air and shaking, the colour eventually faded completely and the spectrum showed no sign of remaining $MV^{\bullet+}$ nor of any new chromophore. Decreasing the sensitizer concentration decreased the rates during both phases, leading to a slower saturation of the detector. Thus, degassing permitted much higher accumulations of $MV^{\bullet+}$. This is due to a secondary generation of $MV^{\bullet+}$ that has previously been attributed to the reduction of MV^{2+} by a deprotonated form of $TEOA^{\bullet+}$ (see later).[4,17] This $TEOA^{\bullet+}$-derived growth is suppressed by O_2 in non-degassed samples (see below).

Applying the rate law

$$\frac{d[MV^{\bullet+}]_t}{dt} = k'_f[MV^{2+}]_t = k'_f[MV^{2+}]_0 - k'_f[MV^{\bullet+}]_t \quad (3)$$

to the degassed data provided $k'_f = 2.04 \pm 0.03 \times 10^{-4}$ s^{-1} over the 200–300 s range of the [Ru] = 5×10^{-5} M data. This dropped to $1.1129(9) \times 10^{-4}$ s^{-1} with the [Ru] = 1×10^{-5} M data over the 100–200 s span. The simple concentration–time slopes ($1.17 \pm 0.01 \times 10^{-6}$ and $6.576 \pm 0.006 \times 10^{-7}$ M s^{-1}, respectively) were virtually identical to the k'_f $[MV^{2+}]_0$ values (with $[MV^{2+}]_0 = 0.006$ M), so that neglecting the time-dependent term of eqn. (3) is justified. The curvilinear phase behaved according to eqn. (2) with the k_d parameters set to 0, providing $k_f = 6.9 \pm 0.1 \times 10^{-4}$ s^{-1} and $k_q = 2.0 \pm 0.3 \times 10^{-2}$ s^{-1} from the initial 150 s of the 5×10^{-5} M data, but these values must be viewed as over- and under-estimates, respectively, because of overlap with the secondary $MV^{\bullet+}$ generation. Indeed, identical but non-degassed samples examined in the same special cuvette confirmed this. Fig. 2 includes a typical run, showing an initial overlap with that from the degassed sample at the same [Ru] value. Analysis by application of eqn. (2) provided $k_f = 5.0 \pm 0.4 \times 10^{-4}$ s^{-1} and $k_q = 4.4 \pm 0.4 \times 10^{-2}$ s^{-1}. The difference in k_f values between degassed and non-degassed samples amounted to k'_f, within experimental error. The overestimation of k_f with the degassed sample was therefore due to the $TEOA^{\bullet+}$-derived, O_2-suppressed growth. By extension, there was little, if any, competitive quenching of the excited state by O_2 in the aerated samples,[18] which would have had the effect of reducing k_f. This also follows from the previously mentioned independence of k_f from instantaneous k_q.

The behaviour of the degassed samples served to illuminate two other phenomena. The first of these was that *certain* aerated samples of $Ru(bpy)_3{}^{2+}$, when kept under prolonged irradiation, underwent a very slow upward drift in A^{600} after reaching the "steady-state plateau", constituting a second, linear growth phase. Fig. 3 depicts illustrative runs. Even after prolonged exposure to light, the spectra revealed no new chromophore other than $MV^{\bullet+}$. The subsequent dark decay resulted in the complete loss of colour with again no new chromophoric species apparent. Kalyanasundaram *et al.* reported no detectable loss of sensitizer nor MV^{2+} upon prolonged irradiation,[4] so sensitizer or MV^{2+} decomposition were not likely responsible for this second growth phase. The concentration–time slope during this second phase was variable, ranging in Fig. 3 from 1.050 ± 0.002 to $2.699 \pm 0.008 \times 10^{-8}$ M s^{-1} (all measured with $r > 0.992$), and the variability suggests that the uncontrolled O_2 concentration was responsible. Importantly, the slopes were strongly and negatively correlated ($r < -0.9999$) with the k_{d2} values measured from the subsequent decays: that is, when the decay phase proceeded more quickly, the linear phase was slower. This correlation is consistent with an incomplete suppression of the TEOA-related growth owing to sub-saturating O_2. An alternative explanation is that the second growth reflects a

† Okura and Kim-Thuan reported that their degassed samples lost $MV^{\bullet+}$ in the dark,[9] but this is likely due to leakage or residual O_2.

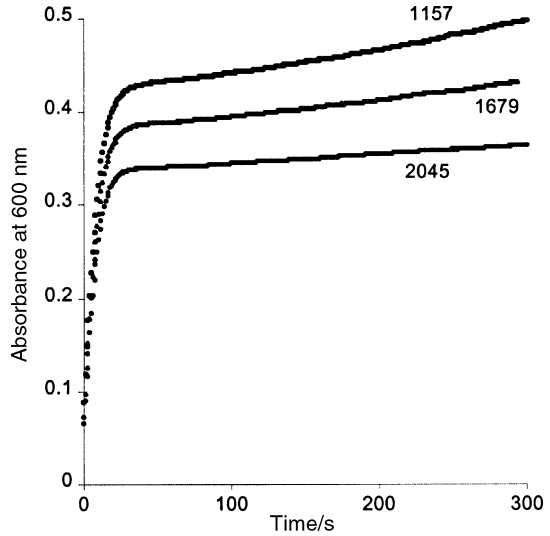

Fig. 3 Plots of A^{600} over time with samples of $[Ru(bpy)_3]^{2+}$, showing upward drift in absorbance, and the k_{d2} values (in $M^{-1}\ s^{-1}$) measured from the subsequent decays. Sample concentrations as in Fig. 1.

decreasing $[O_2]$ over time. This can be discounted because a decreasing $[O_2]$ would have the effect of reducing the instantaneous k_{d2} value and would predict a steady decrease in k_{d2} from one dark decay cycle to the next, which was not observed except by chance. Samples showing this second growth also underwent a slower drift of the absorbance baseline, the amount of which was apparently proportional to the irradiation time. Kalyanasundaram *et al.* reported a darkening of their samples upon prolonged irradiation due to the accumulation of TEOA-derived end-products.[4] While we saw no apparent darkening, such an accumulation can account for the observed drift and that accumulation can only occur in samples where the TEOA-derived generation of $MV^{\bullet+}$ was incompletely suppressed by O_2. With the weaker sensitizer $Ru(ttpy)_2^{2+}$, no such phenomena were observed.

The results with the degassed samples also shed light on the behaviour of non-degassed samples in H_2O. The time courses in H_2O (Fig. 4) were much longer than in CH_3CN (the steady-state value was reached in about 2000 s in the best case) and more complicated, and the $[MV^{\bullet+}]_\infty^{obs}$ values achieved were an order of magnitude higher than in CH_3CN, also leading to detector saturation. Here too, the only new chromophore was $MV^{\bullet+}$. The first $MV^{\bullet+}$ generation under irradiation occurred in several stages, starting with an induction period (A) of variable length, then an initial, rapid but sigmoidal growth phase (B) reaching a plateau within the next 100 s, as in CH_3CN. The plateau level drifted gently upward over the course of about 200 s, followed by a second, prolonged sigmoidal rise (C) that gently sloped off as A^{600} approached saturation, much as with the degassed samples. After decay in the dark, subsequent irradiations (E) showed only the latter, saturating stage proceeding at the same rate, but with no induction period. The intervening dark decay portions (D) were slower than in CH_3CN but purely linear, that is zeroth-order in $[MV^{\bullet+}]$, and therefore diffusion-limited, and this returned A^{600} to the initial values in 2500–3000 s. The diffusion-limited decay is consistent with the lower solubility of O_2 in H_2O (1.4 mM[19] *vs.* 8.1 mM in CH_3CN[20]). In light of the results with the degassed samples, the initial induction reflects a degassing period where the continuously generated $MV^{\bullet+}$ and $TEOA^{\bullet+}$ undergo rapid reactions with O_2 (see later). This degassing eventually slowed and enabled $MV^{\bullet+}$ to accumulate in sigmoidal fashion, from reduction first by the excited state, then by the accumulating $TEOA^{\bullet+}$, by which time the O_2 was depleted and replenished only by diffusion. Subsequent irradiations were O_2-poor throughout, that is without induction, and the two channels of $MV^{\bullet+}$ generation overlapped. Since the instantaneous k_{d2} was not constant (and unknown) during the first growth (B), no useful kinetic parameters could be calculated therefrom, but we noted that the $MV^{\bullet+}$ yield during this phase was fairly constant from sample to sample [$\chi^{obs} = 0.67(3)\%$, averaged over 3 samples]. The slopes from the second and third irradiations over three samples averaged to $8.2 \pm 0.2 \times 10^{-7}\ M\ s^{-1}$, using data over the first 300 s of growth. Since the $MV^{\bullet+}$ is being generated here in the presence of diffusing O_2, this value is understandably less than that measured with the degassed samples. The $MV^{\bullet+}$ yield achieved during phase B is higher than that achieved in (non-degassed) CH_3CN, and this is consistent with the lower concentrations of O_2 present in H_2O.

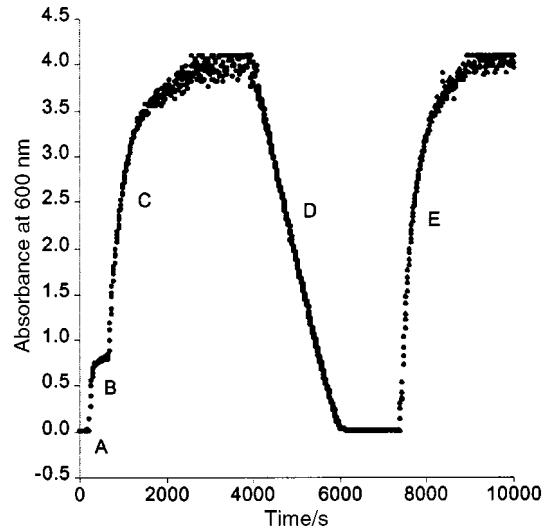

Fig. 4 Plot of A^{600} *vs.* time with $Ru(bpy)_3Cl_2$ in H_2O. Sample concentrations as in Fig. 1 ($MVCl_2$ used).

Very similar behaviour was found in 4 : 1 CH_3CN–H_2O, with a longer induction period A (nearly 800 s), again appearing only on the first irradiation cycle, but no detectable first climb B. The longer induction period reflects the longer degassing needed in this solvent, owing to its greater O_2 content than is achieved in pure H_2O.

Discussion

The reactions at work here have been mostly studied in H_2O, but not in the presence of air nor, except in some cases, under continuous irradiation. The reaction of $MV^{\bullet+}$ with O_2 in H_2O has also been studied separately,[21,22] but not in CH_3CN. This section analyzes the complex set of reactions involved to engender the remarkably simple kinetic model that fits our observations.

General considerations

From flash photolysis studies in H_2O,[4,13] $MV^{\bullet+}$ is known to accumulate by oxidative quenching as follows: the ground-state sensitizer, represented by Ru^{II} in eqn. (4), is promoted by light to its triplet excited state, represented by Ru^{II*}, *via* intersystem crossing from a singlet state. The photophysical details of this process have been reviewed.[16] {Here, k_4 is not a true rate constant but a function of the constant light flux I_0, light absorption characteristics (λ, ε) and quantum yield ϕ for the excitation, but $k_4[Ru^{II}]_t$ can substitute for ϕI_0 at low chromophore concentrations.}[9] The excited state can return to the ground state and the value of k_{-4} is $1/\tau$, which will vary with solvent and $[O_2]$. The available excited state can be quenched by electron transfer to MV^{2+} [eqn. (5)], but this competes with the reverse (back) reaction between the oxidized sensitizer (Ru^{III}) and $MV^{\bullet+}$, which regenerates the starting materials

[eqn. (6)]. The TEOA, present in large excess, competitively traps Ru^{III} by pH-dependent reduction [eqn. (7)] to allow $MV^{\bullet+}$ to accumulate. Rate constants have been obtained for the reactions in eqn. (5)–(7) in H_2O.[4,9,23,24]

$$Ru^{II} \underset{k_{-4}}{\overset{k_4}{\rightleftharpoons}} Ru^{II*} \quad (4)$$

$$Ru^{II*} + MV^{2+} \xrightarrow{k_5} Ru^{III} + MV^{\bullet+} \quad (5)$$

$$Ru^{III} + MV^{\bullet+} \xrightarrow{k_6} Ru^{II} + MV^{2+} \quad (6)$$

$$Ru^{III} + TEOA \xrightarrow{k_7} Ru^{II} + TEOA^{\bullet+} \quad (7)$$

The fate of the $TEOA^{\bullet+}$ product is less well known, and is pH-dependent. In (degassed) alkaline H_2O solutions, the initial rapid build-up of $MV^{\bullet+}$ after a laser pulse is followed by a slower growth occurring over several tens of μs attributable to a reduction of MV^{2+} by a deprotonated form of $TEOA^{\bullet+}$ [eqn. (8) and (9)] to constitute a second pathway of $MV^{\bullet+}$ generation:

$$TEOA^{\bullet+} \overset{K_{a8}}{\rightleftharpoons} H_{-1}TEOA^{\bullet} + H^{+} \quad (8)$$

$$H_{-1}TEOA^{\bullet} + MV^{2+} \xrightarrow{k_9} MV^{\bullet+} + H_{-1}TEOA^{+} \quad (9)$$

(The $H_{-1}TEOA^{+}$ product is a protonated aldehyde or an iminium ion, depending on the regiochemistry of deprotonation, whose fates in CH_3CN are unknown.) In acidic H_2O, on the other hand, the $MV^{\bullet+}$ decays over several tens of μs because the reaction in eqn. (9) is suppressed and $TEOA^{\bullet+}$, itself a mild oxidant, provides an alternate pathway for the quenching of $MV^{\bullet+}$:

$$MV^{\bullet+} + TEOA^{\bullet+} \xrightarrow{k_{10}} MV^{2+} + TEOA \quad (10)$$

(The value of k_9 has been variously determined to be 2.5×10^6[4] and 2.7×10^9 M^{-1} s^{-1}.[25]) Entirely analogous pH-dependent behaviour was observed when H_4EDTA was used as a sacrificial reductant.[26] With cysteine, however, there is no process analogous to eqn. (9), but the secondary quenching of $MV^{\bullet+}$ analogous to the reaction given in eqn. (10) could be prevented by a deprotonation analogous to eqn. (8) in alkaline buffer.[4]

Although we cannot readily translate pH and pK_a values to non-aqueous solutions, our CH_3CN solutions are nevertheless basic. No value for k_{10} is available (it is estimated to be of the order of 10^9 M^{-1} s^{-1})[17] but previous work[4] makes clear that eqn. (8) and eqn. (9) overtake eqn. (10) at alkaline pH, so that neglecting eqn. (10) is justified in the present context. Eqn. (8) and eqn. (9) therefore account for the second growth phase that was prominent in our degassed samples and in H_2O (Fig. 2 and 4), as well as for the much less prominent second growth phase seen in some of the non-degassed samples of $Ru(bpy)_3^{2+}$ (Fig. 3). That no detectable second growth phase or baseline drift occurred with the weaker sensitizer $Ru(ttpy)_2^{2+}$ was likely because the levels of $TEOA^{\bullet+}$ achieved were too low and the inhibition by O_2 too easy. Possible mechanisms for this inhibition include an electron transfer from $H_{-1}TEOA^{\bullet}$ or the formation of a peroxide.

Under continuous irradiation, the Ru will achieve steady-state values, as was assumed by Okura and Kim-Thuan.[9] Indeed, eqn. (4) and (5) lead to

$$\frac{d[Ru^{II*}]_t}{dt} = k_4[Ru^{II}]_t - [Ru^{II*}]_t(k_{-4} + k_5[MV^{2+}]_t)$$

Steady-state $[Ru^{II*}]_t$ will be achieved when

$$[Ru^{II*}]_\infty = \frac{k_4([Ru^{II}]_0 - [Ru^{III}]_\infty)}{k_4 + k_{-4} + k_5([MV^{2+}]_0 - [MV^{\bullet+}]_\infty)} \approx \frac{k_4[Ru^{II}]_0}{k_4 + k_{-4} + k_5[MV^{2+}]_0}$$

is constant. This will hold true because only $<1\%$ of MV^{2+} is ever transformed to the radical ($[MV^{2+}]_0 \gg [MV^{\bullet+}]_t$), and because no significant amount of Ru^{III} accumulates in the presence of accumulating $MV^{\bullet+}$ [by eqn. (6)] and a large excess of TEOA by eqn. (7), whence $[Ru^{II}]_0 \gg [Ru^{III}]_t$. Similarly, eqn. (5)–(7) lead to

$$\frac{d[Ru^{III}]_t}{dt} = k_5[Ru^{II*}]_t[MV^{2+}]_t - [Ru^{III}]_t(k_6[MV^{\bullet+}]_t + k_7[TEOA]_t)$$

With experimental values of k_5 (5×10^8 in H_2O[4] or 2.4×10^9 in CH_3CN[27] or $1.9–2.3 \times 10^9$ M^{-1} s^{-1} in H_2O–CH_3CN mixtures[28]), k_6 (2.4×10^9 to 1.1×10^{10} M^{-1} s^{-1} in H_2O, depending on ionic strength)[4,23] and k_7 (4.7×10^7 at pH 9,[4] 2.7×10^7 M^{-1} s^{-1} at pH 8.1[24]), this describes a rapid build-up of $[Ru^{III}]_t$ [by eqn. (5)] that slopes off [by eqn. (6) and (7)] until a steady state is achieved when

$$[Ru^{III}]_\infty = \frac{k_5[Ru^{II*}]_t([MV^{2+}]_0 - [MV^{\bullet+}]_t)}{k_6[MV^{\bullet+}]_t + k_7[TEOA]_t} \approx \frac{k_5[Ru^{II*}]_\infty[MV^{2+}]_0}{k_7[TEOA]_0}$$

is constant. Because $[Ru^{II*}]_t$ becomes constant and $[MV^{2+}]_0 \gg [MV^{\bullet+}]_t$ as discussed above, steady-state $[Ru^{III}]_t$ will occur while $k_7[TEOA] \gg k_6[MV^{\bullet+}]_t$. This inequality is numerically substantiated over the entire course of our experiments, since we used $[TEOA]_0 = 0.05$ M and $[MV^{\bullet+}]_t$ remained $\leqslant 4.5 \times 10^{-5}$ M in our samples.

Curvilinear growth phase

With neglect of eqn. (10) under basic conditions, and before eqn. (9) contributes significantly, the rate law can be written

$$\frac{d[MV^{\bullet+}]_t}{dt} = k_5[Ru^{II*}]_t[MV^{2+}]_t - k_6[Ru^{III}]_t[MV^{\bullet+}]_t = k_f[MV^{2+}]_t - k_q[MV^{\bullet+}]_t \quad (11)$$

With $[Ru^{II*}]_t$ and $[Ru^{III}]_t$ at unknown steady-state values, we write $k_f = k_5[Ru^{II*}]_\infty$ and $k_q = k_6[Ru^{III}]_\infty$. Previous authors have measured only the initial[11–14] or instantaneous[9] rates under continuous irradiation. (At this point, it is worth noting that, using the formalism of Okura and Kim-Thuan,[9] the ratio k_q/k_f corresponds to $k_6[MV^{2+}]_0/k_7[TEOA]_0$. With the values of Table 1, and with $[MV^{\bullet+}]_t \leqslant \chi^{obs}[MV^{2+}]_0$, it can be verified that the inequality which enables $[Ru^{III}]_t$ to achieve a steady state, $k_7[TEOA] \gg k_6[MV^{\bullet+}]_t$, also comfortably holds in CH_3CN.)

Because our experiments did not involve any measure of light intensity, $[Ru^{II*}]_t$ or $[Ru^{III}]_t$, the quantities k_f and k_q cannot be numerically related to the primary rate constants (k_{-4} and k_4 to k_7) that they incorporate, even if ϕ and τ are known, although the observed concentration dependences can be rationalized under the kinetic model (see earlier). The values of k_f and k_q only have meaning in comparisons between sensitizers evaluated under identical conditions, and such comparisons can be made even if ϕ and τ are not known, but the differences between sensitizers in k_f or k_q values cannot be ascribed to any particular cause.

TEOA-related growth phases

With $[Ru^{III}]_t$ constant, eqn. (7) should be pseudo-zeroth order (*i.e.*, linear) while $[TEOA]_0 \gg [Ru^{III}]_t$. There are two drains for $TEOA^{\cdot+}$: aerobic decomposition and MV^{2+} reduction. Both will lead to a steady state.

In air, eqn. (9) is precluded by what must be a faster reaction with O_2. If this is represented by eqn. (12), a pseudo-first order process in the presence of excess O_2,

$$TEOA^{\cdot+} \xrightarrow{k_{12}} \text{decomposition products (DP)} \quad (12)$$

then it can be shown that a steady state will be achieved when

$$[TEOA^{\cdot+}]_t = \frac{k_7[Ru^{III}]_t([TEOA]_0 - [DP]_t)}{k_7[Ru^{III}]_t + k_{12}}$$

is constant, which will be true at constant $[Ru^{III}]_t$ and while TEOA remains largely unconsumed ($[TEOA]_0 \gg [DP]_t$). The decomposition of constant $[TEOA^{\cdot+}]_t$ in the presence of excess air will then be at a constant rate.

The absence of air allows eqn. (9) to take place. Since $[H_{-1}TEOA^{\cdot}]_t = K_{a8}[TEOA^{\cdot+}]_t/[H^+]_t$, we write

$$\frac{d[TEOA^{\cdot+}]_t}{dt} = k_7[Ru^{III}]_t([TEOA]_0 - [TEOA^{\cdot+}]_t - K_{a8}[TEOA^{\cdot+}]_t/[H^+]_t) - k_9K_{a8}[TEOA^{\cdot+}]_t \times ([MV^{2+}]_0 - [MV^{\cdot+}]_t)/[H^+]_t$$

This will be zero if

$$[TEOA^{\cdot+}]_t = \frac{k_7[Ru^{III}]_t[TEOA]_0}{k_7[Ru^{III}]_t(1 + K_{a8}/[H^+]_t) + k_9K_{a8}([MV^{2+}]_0 - [MV^{\cdot+}]_t)/[H^+]_t}$$

is constant, which will occur at constant $[Ru^{III}]_t$ and because $[MV^{2+}]_0 \gg [MV^{\cdot+}]_t$, as presented earlier, with the additional proviso that $[H^+]_t$ remains constant, which the buffering effect of a large excess of TEOA will ensure. Then $[H_{-1}TEOA^{\cdot}]_t$ will also be constant. The TEOA-derived $MV^{\cdot+}$ generation [reaction (9)] then becomes pseudo-zeroth-order, as observed.

The change in $MV^{\cdot+}$ concentration during the linear growth phase with the degassed samples will be due to reaction (9) and be governed by eqn. (3) with $k'_f = k_9[H_{-1}TEOA^{\cdot}]_\infty$, where the subscript ∞ denotes an unknown steady-state concentration. At sub-saturating or diffusion-controlled $[O_2]$, the second, linear growth phase is then the result of a competition between nearly invariant $[MV^{2+}]_t$ and nearly constant $[O_2]_t$ for the nearly constant (but lower) $[H_{-1}TEOA^{\cdot}]_t$, and the slope k'_f has the same meaning.

In principle, it should be possible to compare sensitizers through k'_f values measured under identical conditions with degassed samples, albeit less conveniently.

Aerobic decay

In H_2O, two very fast reactions of $MV^{\cdot+}$ with O_2 and $O_2^{\cdot-}$ lead to H_2O_2 [eqn. (13) and (14)],[21] which also reacts [eqn. (15)],[22] though much more slowly. Eqn. (15) is precluded in the presence of excess O_2.[22] The rapid disproportionation of $O_2^{\cdot-}$ [eqn. (16)][29] may become competitive under certain conditions.

$$MV^{\cdot+} + O_2 \rightarrow MV^{2+} + O_2^{\cdot-} \quad k_{13} = 7.7 \times 10^8\ M^{-1}\ s^{-1} \quad (13)$$

$$MV^{\cdot+} + O_2^{\cdot-} \rightarrow MV^{2+} + O_2^{2-} \quad k_{14} = 6.5 \times 10^8\ M^{-1}\ s^{-1} \quad (14)$$

$$2MV^{\cdot+} + H_2O_2 \rightarrow MV^{2+} + 2H_2O \quad k_{15} = 2.3 \times 10^3\ M^{-1}\ s^{-1} \quad (15)$$

$$2O_2^{\cdot-} \rightarrow O_2 + O_2^{2-} \quad k_{16} = 1.0 \times 10^6\ M^{-1}s^{-1} \text{ at pH } 6.8 \quad (16)$$

Electrostatic interactions are more important in CH_3CN than in H_2O. The development of charge in the products [eqn. (13) and (14)] or a repulsion between reactants [eqn. (15) and (16)] should slow these reactions in CH_3CN. (For the same reason, any direct quenching of Ru^{II*} by O_2 through electron transfer[18] should also be slower in CH_3CN than in H_2O.)

Two mechanisms can be proposed to explain the dominant second-order dependence of eqn. (1). Trimolecular eqn. (17)

$$2MV^{\cdot+} + O_2 \xrightarrow{k_{17}} 2MV^{2+} + O_2^{2-} \quad (17)$$

is pseudo-second-order so long as $[O_2]_0 \gg [O_2^{2-}]_t$, but this is entropically and electrostatically disfavoured.

Alternatively, we can consider that the reverse of eqn. (13) is more electrostatically favoured than either the forward reaction or the subsequent eqn. (14). If eqn. (13) is reversible in organic solvents [eqn. (18)],

$$MV^{\cdot+} + O_2 \overset{K_{18}}{\rightleftharpoons} MV^{2+} + O_2^{\cdot-} \quad (18)$$

then, at the resulting low steady-state concentrations of $O_2^{\cdot-}$, eqn. (14) can be rate-determining, whence

$$\frac{d[MV^{\cdot+}]_t}{dt} \approx -k_{14}[MV^{\cdot+}]_t[O_2^{\cdot-}]_t = -\frac{k_{14}K_{18}[O_2]_t}{[MV^{2+}]_t}[MV^{\cdot+}]_t^2$$

Because $[MV^{\cdot+}]_t \ll [MV^{2+}]_0$, this is pseudo-second-order while O_2 remains in excess. Then $k_d \approx k_{14}K_{18}[O_2]_0/[MV^{2+}]_0$. Such a mechanistic picture remains tentative until eqn. (13) and (14) can be studied in CH_3CN, but it explains the observations. With the weaker sensitizer, a first-order decay term was found to be non-negligible. This may indicate that another pathway competes at low $[MV^{\cdot+}]_t$ levels, perhaps acting to drain $O_2^{\cdot-}$ [*e.g.*, by eqn. (16)] and reduce the reversibility of eqn. (13).

Aerobic growth phase

Combining eqn. (11) with eqn. (1) while eqn. (9) is aerobically suppressed provides the observed rate law given as eqn. (2).

We used the values of the k_d parameters obtained from the application of eqn. (1) to the decay cycle as fixed constants during the application of eqn. (2) to the irradiated growth cycle, and consistent values of k_f and k_q were thereby obtained. This assumed that $[O_2]$ remained in excess throughout. It was not possible to ensure this in a control experiment by bubbling O_2 in the samples without disturbing the two light paths and without causing the evaporation of CH_3CN. But a relatively constant, excess $[O_2]$ is entirely feasible with stirred samples in a solvent that dissolves appreciable amounts of O_2, and is substantiated by the consistency in the values of k_{d2} from sequential runs with any one sample.

Conclusion

The use of degassed preparations enables a second path of $MV^{\cdot+}$ generation owing to the sacrificial reductant. This second path can mask the intrinsic ability of a photosensitizer to generate $MV^{\cdot+}$ by oxidative quenching. It is inhibited by

O_2 but, in aqueous media, the inhibition causes an effective degassing. Non-degassed CH_3CN solutions are convenient to prepare from sensitizer samples generated by a combinatorial method, and more amenable to the assessment of sensitizer utility for their eventual application in systems where there will be no sacrificial reductant. Even if the attendant aerobic decay of $MV^{\bullet+}$ prevents one from reaching the yields of $MV^{\bullet+}$ that are intrinsically possible with a given sensitizer, the method described here allows one to nevertheless discover that potential by taking account of the aerobic decay. One can measure the appearance of $MV^{\bullet+}$ with routine equipment and non-degassed samples, then analyze the time-dependence with a sound kinetic model. The rate constants from eqn. (2) are reproducible, consistent with the mechanism, and consistent with photosensitization ability. They are also consistent with initial rates. So long as the data from different sensitizers are acquired under identical conditions, the method generates results (k_f, k_q and χ^{theor}) that can be used to compare sensitizers of widely varying ability. It may be possible to devise a similar means of assessing those sensitizers that undergo reductive quenching.[5]

Methodology

Commercial $[Ru(bpy)_3]Cl_2$ was used in H_2O and converted to $[Ru(bpy)_3](PF_6)_2$ by standard techniques for use in CH_3CN. $[Ru(ttpy)_2](PF_6)_2$ was prepared by a literature method.[30]

Non-degassed samples

Disposable, 3 mL polyethylene, 1 cm pathlength cuvettes with square openings were fitted with a short magnetic stirring bar and contained sample CH_3CN solutions (2.5 mL) of the sensitizers (as PF_6^- salts, 4×10^{-5} M), MV^{2+} (as the PF_6^- salt, 9.45×10^{-3} M) and triethanolamine (TEOA, 5×10^{-2} M), assembled from stock solutions by syringe transfers. Experiments in H_2O used $[Ru(bpy)_3]Cl_2$ in aqueous stocks, either alone or in combination with CH_3CN stocks for samples in 4 : 1 CH_3CN–H_2O. To assess the effects of each component, samples were also prepared with each component at 20, 60, 100 or 200% of these values in every possible combination. The cuvettes were placed in the light path of a HP 8452A diode-array spectrophotometer. A Peltier-type cuvette holder provided for thermostatting (to 25 °C) and magnetic stirring (500 rpm) under the control of an HP 89090A controller. The stirring was insufficient to visibly perturb the surface but adequately mixed the solution in the spectrometer's light path for steady absorbance readings while irradiated. Irradiation was from overhead and used a Keystone 1200 slide projector fitted with a 500 W Sylvania bulb, with the bottom of the lens 14 cm above the top of the sample cuvette, and with the light beam focused at the top of the cuvette. Between the light source and the cuvette was clamped a Petri dish containing a 1 cm thick layer of a light filtering (400–600 nm bandpass) solution made from $CuSO_4$ and $Fe(NH_4)(SO_4)_3$.[31] After zeroing the detector in the dark, the absorbance at 600 nm, A^{600} (ε 10 060 M^{-1} cm^{-1} in CH_3CN[32] or 11 300 M^{-1} cm^{-1} in H_2O[33]) was monitored and stored in the memory while the solution was irradiated (every 1 s in CH_3CN, or every 10 s for the slower reactions in H_2O or in 4 : 1 CH_3CN–H_2O) until A^{600} reached a steady maximum, then the decay of A^{600} was similarly monitored after the light source was extinguished. The effect of stray light was gauged but found to be negligible if the room lights were extinguished and the windows curtained.

The A^{600} decay in CH_3CN obeyed the rate law given by eqn. (1). Neglecting k_{d1}, plots of $(1/A_0 - 1/A_t)$ *vs.* time using the first 50–100 data points provided zero-intercept slopes k_{d2}/ε [$r > 0.994$ with $Ru(bpy)_3^{2+}$, > 0.964 with $Ru(ttpy)_3^{2+}$). Otherwise, eqn. (1) was integrated to provide

$$[MV^{\bullet+}]_t = \frac{k_{d1}}{(k_{d2} + k_{d1}/[MV^{\bullet+}]_0)e^{k_{d1}t} - k_{d2}}$$

The A^{600} values calculated from this with trial values of the k parameters were fitted to the observed values over the entire decay period by variation of the k parameters using standard, non-linear least-squares iteration, which made use of analytical derivatives to construct the Hessian matrix.

The rate law applying to irradiated samples, eqn. (2), integrates and rearranges to

$$[MV^{\bullet+}]_t = -\frac{Q \tanh(P - Qt/2) + k_f + k_q + k_{d1}}{2k_{d2}}$$

where $P = \tanh^{-1}\{-(2[MV^{\bullet+}]_0 + k_f + k_q + k_{d1})/Q\}$ and $Q = [(k_f + k_q + k_{d1})^2 + 4k_f k_{d2}]^{1/2}$. A non-linear least-squares treatment as above was carried out over the first 100 s [for $Ru(bpy)_3^{2+}$] or 150 s [for $Ru(ttpy)_3^{2+}$]. The inverted Hessian matrix provided statistical estimates of the uncertainties in the calculated parameters and of their covariance. Multiple minima arose if all k parameters were estimated in this manner, because of strong covariance between the quenching rate constants. Though the k_f values were robust, the global-minimum values of k_q and k_{d2} were also strongly dependent on the range of data chosen, even if weighting (as described below) was applied to counteract this, because the determination of k_{d2} relies more strongly on the high-A^{600} data. Since the k_{d2} values obtained from the dark decay data were fairly constant from cycle to cycle, the values of k_f and $(k_q + k_{d1})$ were instead calculated without difficulty if k_{d2} was fixed at the value afforded by a prior analysis of the subsequent dark decay. The k_q was then extracted using the previously determined value of k_{d1}.

To minimize the dependence of the results on the range of data used, the data were weighted according to their expected variances arising from the propagation of errors in the A^{600} measurements (instrumental noise), in ε and in k_{d2}. The weight w_i of the ith data point was set with

$$w_1^{-1} = \sigma^2(A_i^{calc}) = \sigma^2(A^{obs}) + \left\{\frac{dA_i^{calc}}{d\varepsilon}\,\sigma(\varepsilon)\right\}^2 + \left\{\frac{dA_i^{calc}}{dk_{d2}}\,\sigma(k_{d2})\right\}^2$$

The $\sigma(A^{obs})$ component was the standard deviation of A^{600} estimated over 100 points in the steady-state, plateau region or from the linear growth regions (typically at < 0.005 absorbance units), $\sigma(\varepsilon)$ was estimated at 5% of the ε value, given the variation appearing in the literature,[32] and $\sigma(k_{d2})$ was available from the earlier determination of k_{d2}. The latter term had little effect and could be neglected, but the second term reduced the impact of the high-A^{600} data, whose corresponding A^{calc} values are most prone to an error in ε. Excellent fits were obtained with standard errors in the calculated A^{600} values, typically $< 2\%$. It was noted that neglecting the second-order quenching term ($k_{d2} = 0$) gave very poor fits, as the curvature in the simulated data was not acute enough, while neglecting the first-order quenching term ($k_q = 0$) produced too severe a curvature. We also noted that $k_q \gg k_{d1}$.

Three samples of each sensitizer were used. Each sample was taken through three cycles of growth and decay, and weighted averaged values of k_f and k_q and their standard deviations were calculated therefrom, using as weights the uncertainties in each cycle's values obtained from the diagonal elements of the inverted Hessian matrix. The final value reported for any one sensitizer preparation was the average of the three such averages, each weighted by its standard deviation. The maximum radical concentrations ($[MV^{\bullet+}]_\infty^{obs}$) were similarly averaged.

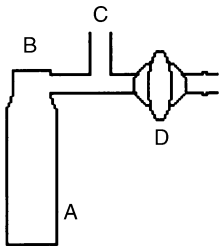

Fig. 5 Sealable cuvette for degassed samples.

Degassed samples

A sealable cuvette (Fig. 5) was constructed from square glass tubing (A, 1 cm inner width) fitted with a flat bottom and fused to a short, capped cylindrical piece (B, 8 mm diameter) which bore, on its side, a T-joint with one arm (C) oriented vertically and the other fused to an in-line stopcock (D). The bar magnet and sample components were introduced through the vertical arm, which was then capped with a septum. (To slow the increase in $MV^{\bullet+}$, the $[MV^{2+}]_0$ was reduced to 0.006 M in these samples.) The contents were protected from light with aluminum foil, then degassed (three freeze–pump–thaw cycles) and back-filled with Ar. The stopcock was then kept closed and the assembly was transferred to the spectrometer cell holder for measurement as above after removing the foil in the dark. Control samples were also prepared in the same cuvette without degassing and with the side-arm kept open.

Acknowledgement

The authors thank the Natural Sciences and Engineering Research Council (Canada) for funding.

References

1 A. Juris, V. Balzani, F. Barigelletti, S. Campagna, P. Belser and A. von Zelewsky, *Coord. Chem. Rev.*, 1988, **84**, 85; V. Balzani, F. Barigelletti and L. De Cola, *Top. Curr. Chem.*, 1993, **159**, 1.
2 M. Sieler, H. Durr, I. Willner, E. Joselvich, A. Doron and J. F. Stoddart, *J. Am. Chem. Soc.*, 1994, **116**, 3399.
3 K. Kalyanasundaram, *Photochemistry of Polypyridine and Porphyrin Complexes*, Academic Press, London, 1992.
4 K. Kalyanasundaram, J. Kiwi and M. Grätzel, *Helv. Chim. Acta*, 1978, **61**, 2720.
5 Review: D. J. Cole-Hamilton and D. W. Bruce, in *Comprehensive Coordination Chemistry*, ed. G. Wilkinson, R. D. Gillard and J. A. McCleverty, Pergamon, Oxford, 1987, vol. 6, pp. 487–540.
6 K. Kalyanasundaram, *Photochemistry of Polypyridine and Porphyrin Complexes*, Academic Press, London, 1992, ch. 11.
7 P. Keller and A. Moradpour, *J. Am. Chem. Soc.*, 1980, **102**, 7193; O. Johansen, A. Launikonis, J. W. Loder, A. W. H. Mau, W. H. F. Sasse, J. D. Swift and D. Wells, *Aust. J. Chem.*, 1981, **34**, 981.
8 L. J. Fitzpatrick, H. A. Goodwin, A. Launikonis, A. W. H. Mau and W. H. F. Sasse, *Aust. J. Chem.*, 1983, **36**, 2169.
9 I. Okura and N. Kim-Thuan, *J. Chem. Soc., Faraday Trans. 1*, 1981, **77**, 1411.
10 M. Kaneko, A. Yamada and Y. Kurimura, *Inorg. Chim. Acta*, 1980, **45**, L73.
11 K. Mandal and M. Z. Hoffman, *J. Phys. Chem.*, 1984, **88**, 185.
12 H. Sun and M. Z. Hoffman, *J. Phys. Chem.*, 1994, **98**, 11719.
13 M. Georgopoulos and M. Z. Hoffman, *J. Phys. Chem.*, 1991, **95**, 7717.
14 Y.-S. Kim, S. McNiven, K. Ikebukuro and I. Karube, *Photochem. Photobiol.*, 1997, **66**, 180.
15 J.-P. Sauvage, J.-P. Collin, J.-C. Chambon, S. Guillerez, C. Coudret, V. Balzani, F. Barigelletti, L. De Cola and L. Flamigni, *Chem. Rev.*, 1994, **94**, 993.
16 K. Kalyanasundaram, *Coord. Chem. Rev.*, 1982, **46**, 159.
17 S.-F. Chan, M. Chou, C. Creutz and N. Sutin, *J. Am. Chem. Soc.*, 1981, **103**, 369.
18 K. Kalyanasundaram, *Photochemistry of Polypyridine and Porphyrin Complexes*, Academic Press, London, 1992, pp. 155–156.
19 W. F. Linke, *Solubilities of Inorganic and Metal-Organic Compounds*, American Chemical Society, Washington, DC, 1965, vol. 2; *IUPAC Solubility Data Series*, ed. R. Battino, Pergamon Press, Oxford, 1981, vol. 7; J. A. Dean, *Lange's Handbook of Chemistry*, 15th edn., McGraw-Hill Inc., New York, 1999.
20 D. T. Sawyer, G. Chiericato, Jr., C. T. Angelis, E. J. Nanni, Jr. and T. Tsuchiya, *Anal. Chem.*, 1982, **54**, 1720.
21 J. A. Farrington, M. Ebert, E. J. Land and K. Fletcher, *Biochim. Biophys. Acta*, 1973, **314**, 372.
22 R. N. F. Thorneley, *Biochim. Biophys. Acta*, 1974, **333**, 487.
23 M. Z. Hoffman and D. R. Prasad, *J. Photochem. Photobiol. A*, 1990, **54**, 197.
24 G. M. Brown, S.-F. Chan, C. Creutz, H. A. Schwarz and N. Sutin, *J. Am. Chem. Soc.*, 1979, **101**, 7638.
25 D. R. Prasad and M. Z. Hoffman, *J. Am. Chem. Soc.*, 1986, **108**, 2568.
26 P. Keller, A. Moradpour, E. Amouyal and H. B. Kagan, *Nouv. J. Chim.*, 1980, **4**, 377.
27 F. Boletta, M. Maestri and V. Balzani, *J. Phys. Chem.*, 1976, **80**, 2499.
28 H. Sun, A. Yoshimura and M. Z. Hoffman, *J. Phys. Chem.*, 1994, **98**, 5058.
29 D. Behar, G. Czapski, J. Rabani, L. M. Dorfman and H. A. Schwarz, *J. Phys. Chem.*, 1970, **74**, 3209.
30 J.-P. Collin, S. Guillerez, J.-P. Sauvage, F. Barigelletti, L. De Cola, L. Flamigni and V. Balzani, *Inorg. Chem.*, 1991, **30**, 4230.
31 W. W. Wladimiroff, *Photochem. Photobiol.*, 1966, **5**, 243.
32 E. M. Kosower and J. L. Cotter, *J. Am. Chem. Soc.*, 1964, **86**, 5524.
33 P. A. Trudinger, *Anal. Biochem.*, 1970, **36**, 222.